Bioorganic Chemistry 114 (2021) 105079

Contents lists available at ScienceDirect

Bioorganic Chemistry

journal homepage: www.elsevier.com/locate/bioorg

Synthesis, *in vitro* biological investigation, and molecular dynamics simulations of thiazolopyrimidine based compounds as corticotrophin releasing factor receptor-1 antagonists

Hossam R. Elgiushy [a,h], Nageh A. Abou-Taleb [a], George G. Holz [b], Oleg G. Chepurny [b], Ioannis Pirmettis [c], Sotirios Kakabakos [c], Vlasios Karageorgos [d], George Liapakis [d], Amgad Albohy [e], Khaled A.M. Abouzid [f,g,*], Sherif F. Hammad [a,h,*]

[a] Pharmaceutical Chemistry Department, Faculty of Pharmacy, Helwan University, Ain Helwan 11795, Cairo, Egypt
[b] Department of Medicine, SUNY Upstate Medical University, Syracuse, NY, USA
[c] Institute of Nuclear & Radiological Sciences & Technology, Energy & Safety, National Centre for Scientific Research "Demokritos", Athens, Greece
[d] Department of Pharmacology, School of Medicine, University of Crete, Voutes, 71003, Heraklion, Crete, Greece
[e] Department of Pharmaceutical Chemistry, Faculty of Pharmacy, The British University in Egypt (BUE), El-Sherouk City, Suez Desert Road, Cairo 11837, Egypt
[f] Pharmaceutical Chemistry Department, Faculty of Pharmacy, Ain Shams University, Abbassia 11566, Cairo, Egypt
[g] Department of Organic and Medicinal Chemistry, Faculty of Pharmacy, University of Sadat City, Sadat City, Egypt
[h] Basic and Applied Sciences Institute, Egypt-Japan University of Science and Technology (E-JUST), New Borg El-Arab City, 21934 Alexandria, Egypt

ARTICLE INFO

Keywords:
CRFR1 antagonists
Thiazolo[4,5-*d*]pyrimidine
Scaffold hopping
Molecular dynamics simulation

ABSTRACT

Corticotrophin releasing factor receptor-1 (CRFR1) is a potential target for treatment of depression and anxiety through modifying stress response. A series of new thiazolo[4,5-*d*]pyrimidine derivatives were designed, prepared and biologically evaluated as potential CRFR1 antagonists. Four compounds produced more than fifty percent inhibition in the [^{125}I]-Tyr^{0}-sauvagine specific binding assay. Assessment of binding affinities revealed that compound (3-(2,4-dimethoxyphenyl)-7-(dipropylamino)-5-methylthiazolo[4,5-*d*]pyrimidin-2(3*H*)-one) **8c** was the best candidate with highest binding affinity (K_i = 32.1 nM). Further evaluation showed the ability of compound **8c** to inhibit CRF induced cAMP accumulation in a dose response manner. Docking and molecular dynamics simulations were used to investigate potential binding modes of synthesized compounds as well as the stability of **8c**-CRFR1 complex. These studies suggest similar allosteric binding of **8c** compared to that of the co-crystalized ligand CP-376395 in 4K5Y pdb file.

1. Introduction

Corticotrophin releasing factor CRF (also known as corticotrophin releasing hormone, CRH) is a peptide hormone that regulates body response to stress and is composed of 41 amino acids [1]. It was initially described and characterized by Vale in 1981 [2]. CRF is overexpressed in the hypothalamic paraventricular nucleus part of the brain [3]. Elevated central CRF levels are associated with several diseases including anxiety, depression as well as other neurodegenerative disorders [4–6]. CRF is the principal mediator for stress stimulants on the hypothalamic-pituitary-adrenocortical (HPA) axis. CRF effect takes place via the release of adrenocorticotrophic hormone (ACTH) leading to the release of adrenocortical steroids and stress response [7–9]. CRF receptors are type B G-protein coupled receptors (GPCR) and include CRFR1 and CRFR2 [10–12]. CRFR1 is expressed throughout the brain, and found mainly on the anterior pituitary mediating the effects of CRF on ACTH release [3,8,11,13]. Extensive studies clearly revealed that CRFR1 is pivotal in initiating and provoking stress response and anxiety related behaviors [5,14–20]. This crucial role in mediating stress response at very early stages made CRFR1 a highly promising target for the development of novel class of stress related medications. Non-peptide small molecule antagonists of CRFR1 are investigated for treatment of stress related disorders and other correlated neurodegenerative disorders [1,21,22]. Examples of non-peptide small molecule

* Corresponding authors at: Pharmaceutical Chemistry Department, Faculty of Pharmacy, Ain Shams University, Abbassia 11566, Cairo, Egypt (K.A.M. Abouzid). Pharmaceutical Chemistry Department, Faculty of Pharmacy, Helwan University, Ain Helwan 11795, Cairo, Egypt (S.F. Hammad).
E-mail addresses: khaled.abouzid@pharma.asu.edu.eg (K.A.M. Abouzid), sherif.hammad@ejust.edu.eg (S.F. Hammad).

https://doi.org/10.1016/j.bioorg.2021.105079
Received 10 April 2021; Received in revised form 3 June 2021; Accepted 7 June 2021
Available online 10 June 2021

CRFR1 antagonists proved effective anxiolytic and antidepressant in animal models [12] are illustrated in Fig. 1. Moreover, the crystal structure of CRFR1 in complex with the non-peptide antagonist CP-376395 was reported (PDB ID: 4K5Y) revealing allosteric inhibitory effect of non-peptide CRFR1 antagonists at the transmembrane domain (TMD) [23].

1.1. Design and rationale

Analysis of different non-peptide CRFR1 antagonists reveals four basic pharmacophoric requirements. These include mono-, bi- or tricyclic central scaffold with proton accepting nitrogen atom essential for hydrogen bonding, a methyl substitution on the carbon adjacent to the essential nitrogen atom, an orthogonal aromatic ring and a non-bulky mono- or dialkyl amino group [24]. The reported crystal structure of CRFR1 bound to non-peptide antagonist CP-376395 (PDB ID: 4K5Y) supports these pharmacophoric requirements and provided a clear identification of the binding site. Non-peptide CRFR1 antagonists were found to be allosteric inhibitors and their binding pocket is located between 3rd, 5th and 6th transmembranal loops. This binding mode prevents conformational changes of the receptor that are required for the binding of CRF [23]. In addition, the hydrogen bond acceptor nitrogen was found to interact with N283.

In this study we aim to design and synthesize novel CRFR1 antagonist. Our design is based on scaffold hopping and replacing of the central pyridine ring with thiazolo[4,5-*d*]pyrimidine ring system while maintaining the main pharmacophoric features of CP-376395 Fig. 2.

Our designed CRFR1 antagonists shown in Fig. 3 maintain all the aforementioned essential pharmacophoric features. Selection of thiazolo [4,5-*d*]pyrimidine as core scaffold was tempted by previous successful approaches for thiazolo[4,5-*d*]pyrimidine based CRFR1 antagonists [25–27]. The alkyl amino groups were selected carefully with a maximum of four carbon chain based on previous 3D QSAR model [24]. 2,4-Dimethoxyphenyl was carefully selected as the pendent ring where the *ortho*-methoxy group maintains the required orthogonality and the two methoxy groups provide lipophilicity-balancing effect beside being two H-bond accepting sites.

In addition, our target compounds are intended to be used as drugs and to work at the brain level so we decided to study drugability of synthesized compounds and their ability to cross the blood brain barrier (BBB) [28]. Several descriptors can be used to predict drug likeness and ability of molecules to cross BBB such as lipophilicity (expressed as logP value), topological polar surface area (tPSA), molecular weight, number of hydrogen bond donors and acceptors [29,30]. Herein we used Lipinski's rule of five for drug likeness to predict drugability of the new chemical entities [31]. This rule states that drug-like molecules should have a maximum of 1 violation of the following criteria: logP value does not exceed 5, molecular weight does not exceed 500, number of hydrogen bond donor does not exceed 5 and number of hydrogen bond acceptors does not exceed 10. **Table SI-1** summarizes drug-likeness of target molecules using Lipinski's rule of five compared to reference CRFR1 antagonists. Obtained values were calculated through SwissADME server [32].

2. Results and discussion

2.1. Chemistry

Reagents and conditions: (a) CS_2 (1.2 equivalents)/ k_2CO_3 (2 equiv.) aqueous medium-stirring 10–12 h. trichlorotriazine (0.5 equivalents) stirring 0℃, 0.5 h., 6 N NaOH, stirring, 0.5 h. (b) cyanoacetamide (1 equivalent), elemental sulfur (1 equivalent), Triethylamine (1 equivalent),DMF 50-70℃, (c) Acetic anhydride, reflux 140-150℃ (d) $POCl_3$, reflux 180℃, 3–6 h. (e) appropriate dialkyl amine (2 equivalents), ethanol, reflux 70℃, 3–6 h. (f) dimethyl sulfate (2 equivalents), DMF 10 ml, reflux 150℃, 3hrs, and then add10 ml H_2O, triethyl amine few drops. (g) $POCl_3$, reflux 180 ℃, 3–6 h. Appropriate dialkyl amine (2 equivalents), ethanol, reflux 70℃, 3–6 h. (h) appropriate dialkyl amine (2

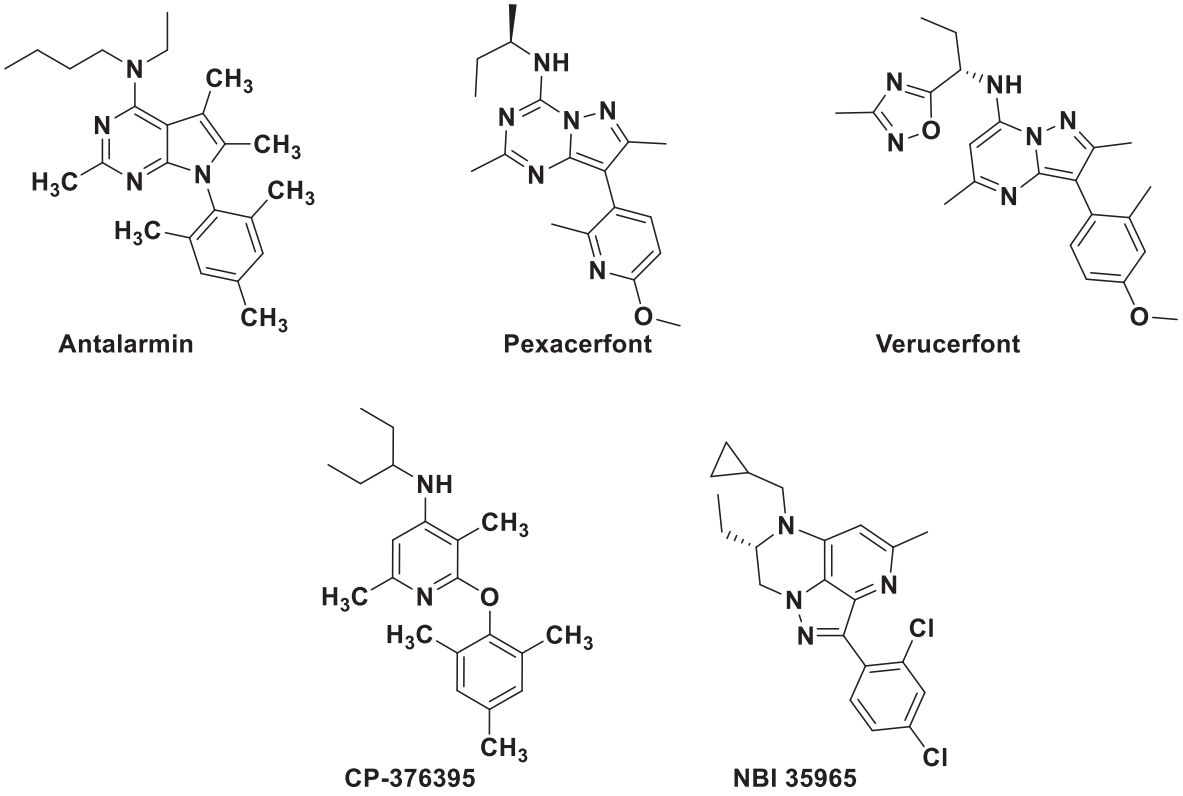

Fig. 1. Examples of non-peptide small molecule CRFR1 antagonists.

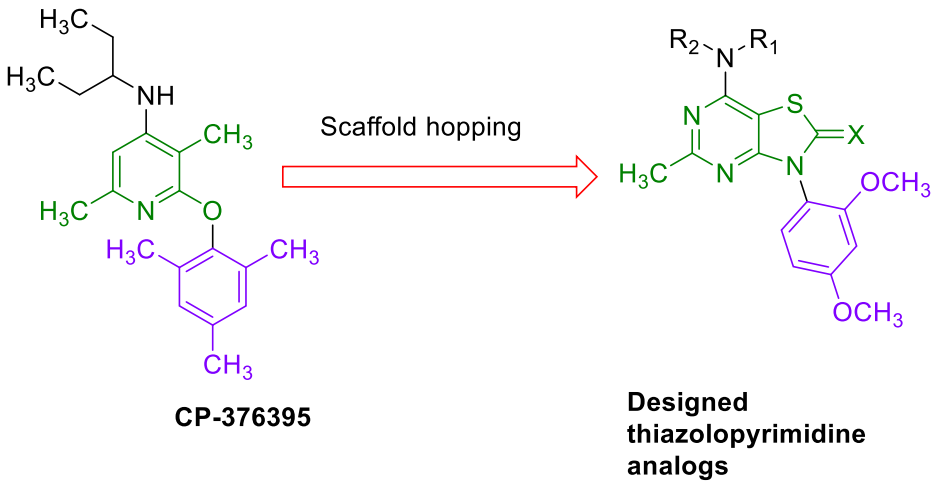

Fig. 2. Design of the target molecules applying scaffold hopping strategy.

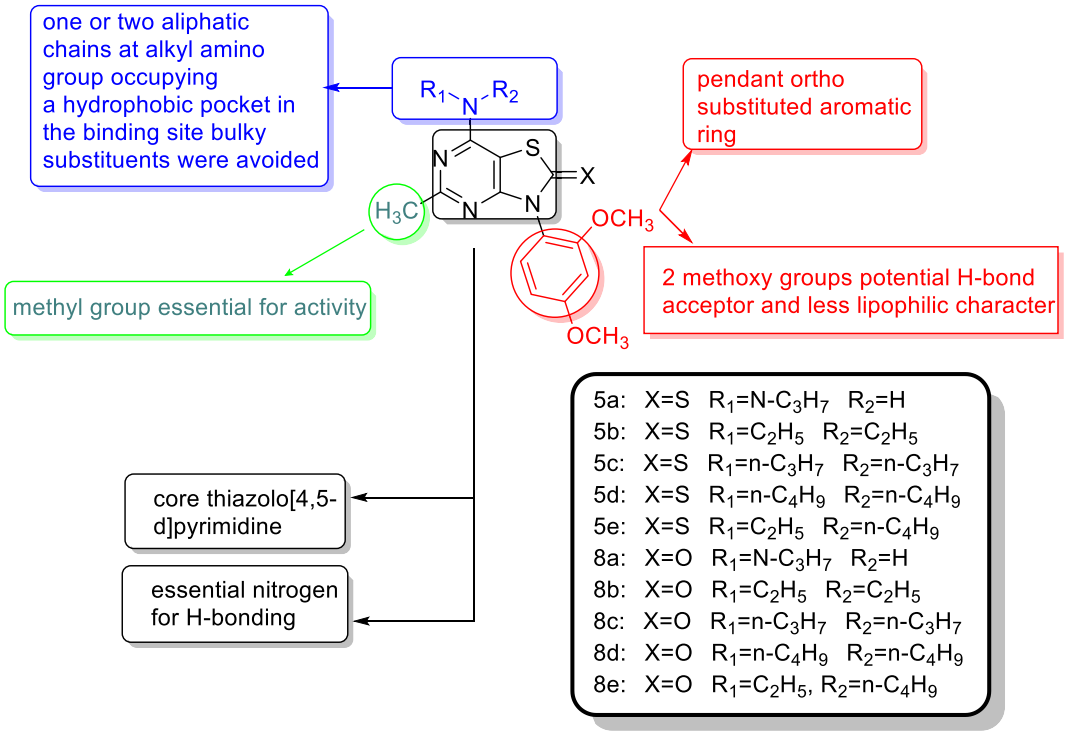

Fig. 3. Target CRFR1 antagonist molecules **5a-e** and **8a-e.**

equivalents), ethanol, reflux 70℃, 3–6 h.

The adopted synthetic pathway is illustrated in scheme 1. Compounds **1**,**2**,**3**,**6** and **7** were prepared and characterized as we previously reported [33]. Both compounds **4** and **7** are reactive towards nucleophilic substitution at *C7*, this is attributed to the presence of imidoyl chloride moiety (Cl-C = NR) [34]. Thus, target compounds **5a-e** were obtained via gentle reflux with two equivalents of appropriate amine. The formation of **5a-e** was confirmed via different spectral analyses. For example, for compound **5b** ^{1}H NMR spectrum shows triplet signal at ***δ*** 1.22 ppm integrated to 6 protons with $J = 7.0$ Hz assigned to protons of the terminal symmetrical two CH_3 of the 7-diethylamino, and a multiplet signal at δ 3.60, $J = 7.2$ Hz integrated to four protons assigned to the four protons of two CH_2 of the 7-diethyl amino. ^{13}C NMR showed the appearance of five signals at the aliphatic region including a signal at δ 13.9 ppm corresponding to two (CH_3) of diethyl amino and a signal at δ 42.816 ppm due to two CH_2 of the 7-diethylamino. Mass spectrometry (MS) revealed the molecular ion peak at m/z = 390.54. Similarly, Compounds **8a-e** were obtained from compound **7** via gentle reflux with appropriate amine. The formation of target compounds **8a-e** was also confirmed by different spectral analyses. Taking compound **8d** as example: ^{1}H NMR revealed the appearance of a triplet signal at δ 0.94 ppm integrated to six protons assigned to the protons of the terminal two (CH_3) of 7-dibutyl amino, a multiplet signal at δ1.34 ppm integrated to four protons assigned to the penultimate protons of the two (CH_2) of 7-dibutylamino, a multiplet signal obtained at δ 1.59 ppm assigned to next four protons of the two (CH_2) of 7-dibutyl amino and a multiplet signal at δ 3.54 ppm assigned to four protons assigned to the four protons of two (CH_2-N) of 7-dibutyl amino. ^{13}C NMR revealed the appearance of four signals of the symmetric dibutyl at δ 14.23, 19.86, 25.01, 48.52 ppm. MS spectrum showed the appearance of molecular ion peak at m/z = 429.88.

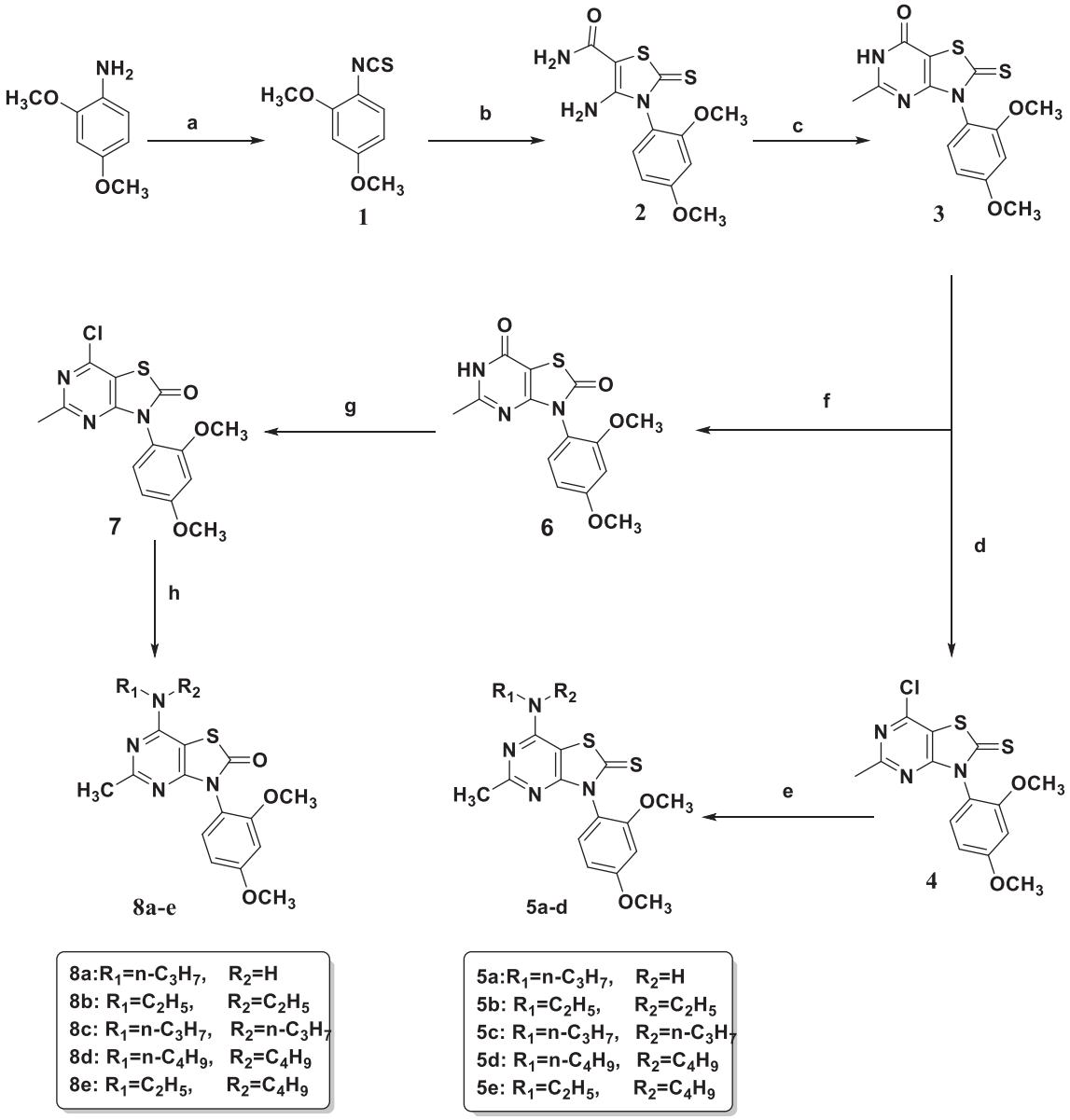

Scheme.1. Synthesis of target compounds **5a-e** and **8a-e.**

2.2. Biological Evaluation:

To test whether the target compounds bind to CRFR1, Tyr^0-sauvagine was radioiodinated and the ability of these compounds to inhibit the specific binding of [^{125}I]-Tyr^0-sauvagine was investigated. The binding affinity of [^{125}I]-Tyr^0-sauvagine was 2.2 nM (-logK_i = 8.66), as determined from homologous competitive binding experiments. The ability of test compounds to inhibit [^{125}I]-Tyr^0-sauvagine binding was tested by determining the specific binding of radioligand (under equilibrium conditions) to membranes from HEK 293 cells stably expressing the CRFR1 in the presence or absence of compounds at a single concentration of 500 nM. Eight final compounds (**5a, 5b**, **5d**, **5e**, **8a, 8b, 8c** and **8d**) were screened for their inhibitory effect**.** Among tested compounds, four compounds have shown less than 50% inhibition which includes **5a**, **8b**, **8d** and **8a** Fig. 4. Compounds **5b**, **5d**, **5e** and **8c**, on the other hand, have shown more than 50% inhibition and were further investigated to determine their inhibitory constant (K_i) for the CRFR1. **5b**, **5d**, **5e** and **8c** were found to bind to the receptor in a dose response manner and with binding affinities of 5-, 6-, 10-, and 2-fold lower than that of antalarmin (Table 1, Fig. 5**,** Fig. 6).

Based on results above, **8c** was found to bind to CRFR1 with higher affinity than other tested compounds and with comparable binding affinity with that of antalarmin. Based on this finding, we tested whether **8c** was able to antagonize CRF-stimulated accumulation of cAMP, which is the secondary messenger that mediates the biological effects resulting from stimulating CRFR1. To accomplish this, we determined its half-maximal inhibitory concentration (or antagonistic potency, - Log IC_{50}) by incubating HEK 293 cells expressing the CRFR1 with 1 nM of CRF in the presence or absence of increasing concentrations of **8c** or antalarmin (control). As shown in Fig. 7, **8c** inhibited CRF-stimulated cAMP accumulation in a dose–response manner, with an antagonistic potency of 2.15 μM. Even though **8c** had similar binding affinity with antalarmin, it was 100 times less potent than antalarmin to inhibit CRF-stimulated cAMP accumulation. Antalarmin inhibited CRF-stimulated cAMP accumulation in a dose–response manner, with an antagonistic potency of 26 nM (Fig. 7). Original FRET data are also shown in the figure on the left side.

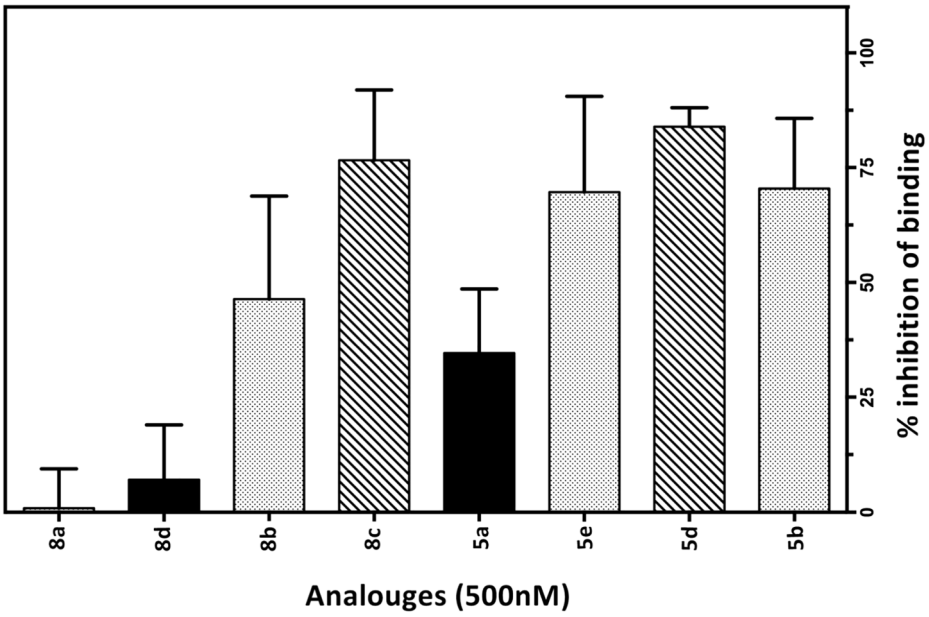

Fig. 4. Screening target compounds for binding to human CRFR1. Inhibition of [^{125}I]-Tyr^{0}-sauvagine specific binding by 500 nM of test compounds was performed.

Table 1
Binding affinities of test compounds for CRFR1.

Analogues*	antalarmin	5b	5d	5e	8c
- LogK$_i$ ± S.E.	7.8 ± 0.15	7.1 ± 0.11	7.0 ± 0.13	6.8 ± 0.13	7.5 ± 0.37
Mean K$_i$ (nM)	16.2	84.5	91.2	169.8	32.1

* K$_d$ of CP-376395 is 7.5 nM [23].

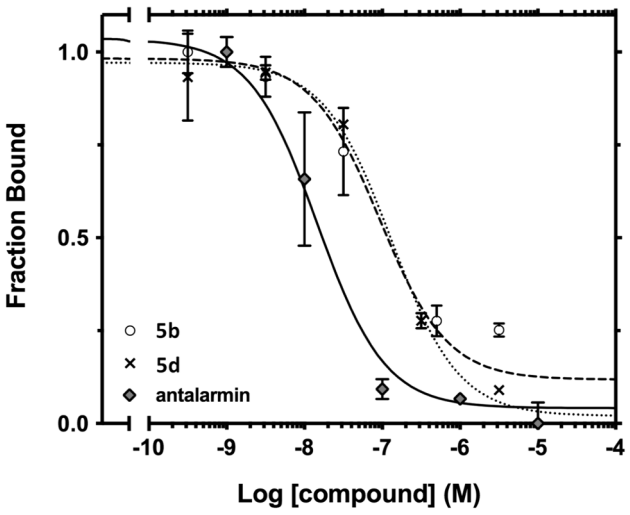

Fig. 5. Competition binding isotherms of **5b**, **5d** and antalarmin to CRFR1.

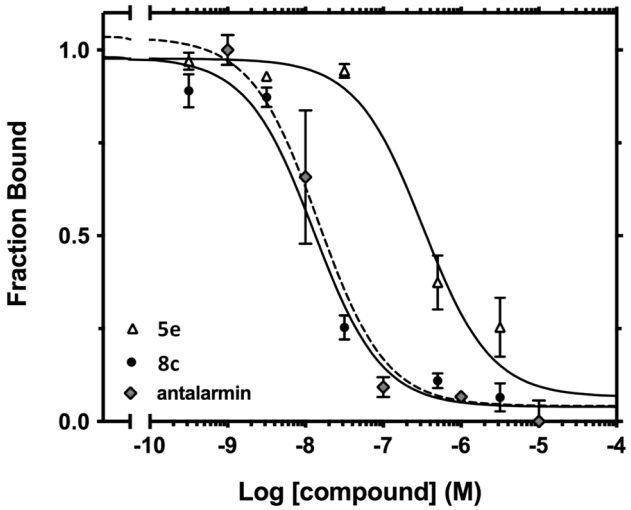

Fig. 6. Competition binding isotherms of **5e**, **8c** and antalarmin to CRFR1.

2.3. Molecular modelling studies

2.3.1. Molecular Docking

Docking was used to study potential binding modes of tested compounds in the allosteric binding site of CRFR1 compared to co-crystallized ligand CP-376395. We tested our compounds along with four known inhibitors that include antalarmin, NBI35965, Pexacerfont and Verucerfont. We also attempted to redock the co-crystalized ligand CP-376395 to validate the docking procedure. We used a large grid box composed of 25^3 Å^3 centered on co-crystalized ligand to explore the whole area around the allosteric site. Redocking of co-crystalized ligand predicted the correct pose with RMSD of 0.635 as calculated by DockRMSD [35] and docking energy of −9.1 kcal/mol. **(Figure SI-1)**

Docking of the four known inhibitors was able to predict a similar pose to the crystal structure in case of the compounds with bicyclic central core motif (Antalarmin, Pexacerfont and Verucerfont) with energies comparable or even better than the monocyclic crystalized CP-376395 (Fig. 8). Docking of the tricyclic inhibitor, NBI35965, was not predicted correctly relative to the co-crystalized ligand and hence its docking energy was low (-8.0 kcal/mol). This might be due to the very rigid structure of NBI35965.

Docking of the tested compounds showed that all of them were able to adapt a similar binding mode to the co-crystalized ligand. All compounds were able to maintain the hydrogen bond between the ring nitrogen and N283 residue. In addition, compounds **5a-e** generally showed smaller scores compared to the series **8a-e.** This suggest that the oxo-derivatives could bind better to CRFR1 when compared to the thioxo derivatives which is consistent with our best hit **8c** being an oxo-

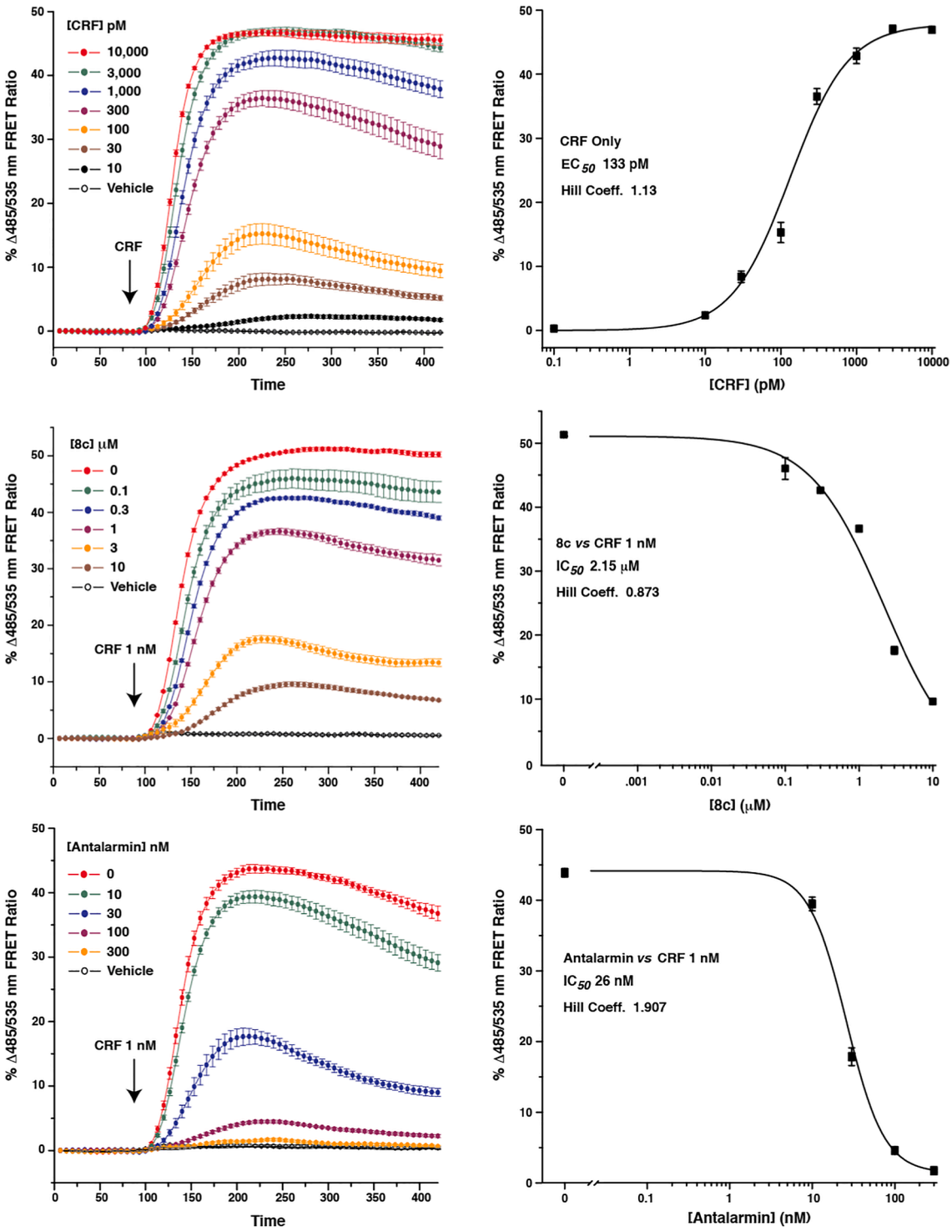

Fig. 7. Inhibition of CRF-stimulated cAMP accumulation by **8c** and antalarmin. Original FRET data are shown on the left side. EC_{50} of CFR is 133 pM as shown in the top raw. 8c (middle raw) and antalarmin (bottom raw) competes with CRF and inhibit CRF-stimulated cAMP accumulation which is detect by FRET ratio.

derivative. Among the first series, compound **5d** had the best docking energy which also the best compound in this series according to the inhibition of [^{125}I]-Tyr0-sauvagine specific binding assay. In case of the second series, docking predicted that compounds **8c-e** have similar binding energies. Compound **8c** is indeed the most active compound but docking was not able to differentiate between the three compounds **8c-e** (Table 2). Considering these findings we decided to further study and compare the stability of **8c** and **8d** complexes as well as co-crystallized ligands using molecular dynamics simulation.

2.3.2. *Molecular dynamics*

Molecular dynamics simulation was performed to investigate the stability of ligand–protein complexes. After preparation steps, CP-376395 crystal structure complexed with CRFR1 was subjected to 50 ns production run along with the apoprotein and **8c** which is the most potent compound. **8c** and the co-crystallized ligands have shown stability in the active site of CRFR1 with ligand heavy atoms RMSD of 2.5–3.0 Å (Table 3 and Fig. 9). Both complexes maintained the hydrogen bond with N283 during most of the run with average distance of 2.25 ±

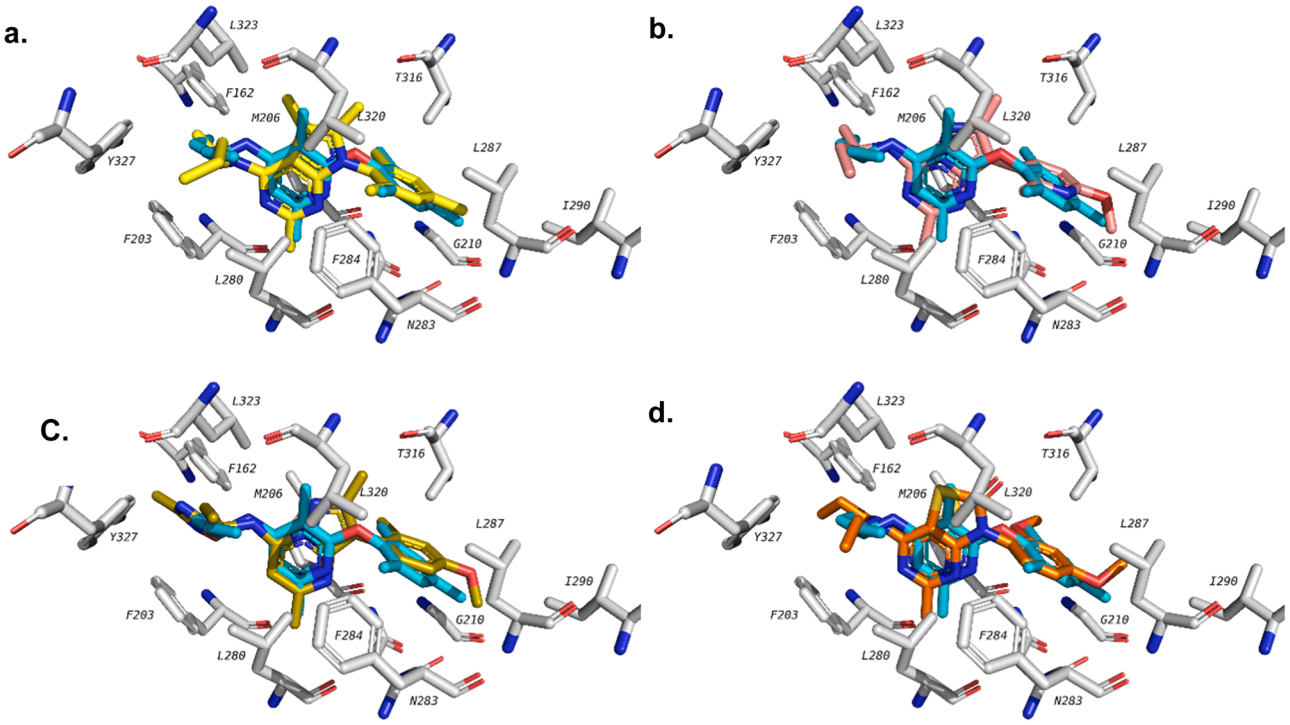

Fig. 8. Docking poses of top compounds compared to the co-crystalized ligand (blue). a, Antalarmin (yellow), b, Pexacerfont (rose), c, Verucerfont (golden) and d, **8c** (orange). (For interpretation of the references to colour in this figure legend, the reader is referred to the web version of this article.)

Table 2
Docking scores of the tested compounds in the allosteric site of CRFR1.

Ligand	Binding Affinity
5a	−8.0
5b	−6.9
5c	−8.5
5d	−8.8
5e	−8.3
8a	−8.3
8b	−8.7
8c	−9.0
8d	−9.1
8e	−9.0
Co-crystalized Ligand	−9.1
Antalarmin	−9.4
NBI35965	−8.0
Pexacerfont	−9.2
Verucerfont	−9.9

Table 3
Average results for the MD production run.

	8c	8d	Control	Apoprotein
Average RMSD of Ligand heavy atoms (Å)	2.52	3.01	3.05	–
Average RMSD of protein (nm)	5.770	5.849	5.836	6.011
Average RMSF of residues (nm)	0.172	0.158	0.146	0.149
Average number of H-Bond	1.82	1.63	0.87	–
Length of hydrogen bond with N283 (Å) (Between hydrogen and nitrogen, N.....H—N)	2.25 ± 0.32	2.31 ± 0.28	2.22 ± 0.20	–
Length of hydrogen bond with N283 (Å)(Between heavy atoms, N.....N)	3.15 ± 0.23	3.20 ± 0.23	3.13 ± 0.16	–
Average Radius of Gyration (Å)	20.04	19.95	20.05	19.82

0.32 Å and 2.22 ± 0.20 Å for **8c** and co-crystalized ligand, respectively. In addition, hydrophobic interactions between ligands (co-crystalized ligand and **8c**) and hydrophobic amino acids in the active site (F203, L280, F284, L287 and L320) are maintained during the whole molecular dynamics run. The average total interaction energy between ligand and protein, calculated by adding short-range Coulombic interaction energy and short-range Lennard-Jones energy, for co-crystalized ligand was found to be − 240.81 ± 0.87 kJ/mol. The total binding energy for **8c** with CRFR1 was stronger compared with the control and was found to be − 306.71 ± 1.54 kJ/mol. Average radius of gyration of all the complexes during the production run was around 20.0 Å. We also performed MM-PBSA calculation for the target complexes with co-crystalized ligand and **8c** over the last 10 ns of the simulation. The results shows that **8c** binding energy with target protein is more than that of co-crystalized ligand with about 27 KJ/mol. The full energy components of the MM-PBSA calculation are shown in table 4.

We were also interested to investigate the effect of elongating the dialkyl amino substitution that leads to a large reduction in inhibitory effect when extending the *n*-propyl of **8c** to *n*-butyl in case of **8d** for example. To study that effect, **8d** complex with CRFR1 was also run for 50 ns. The RMSD of ligand heavy atoms was slightly higher compared to **8c** (table 3). In addition, a plot of protein RMSD compared to crystal structure shows higher fluctuation of the **8d** complex especially during the period of 25–40 ns of the production run (Fig. 10) which might suggest the relative instability of the complex. Also, the average number of hydrogen bonds is less in **8d** and the average distance of hydrogen bond with N283 (2.31 ± 0.28 Å) is slightly longer. All these factors suggest that binding of **8d** is weaker compared to **8c** as have been seen in the biological assay which suggests that the N,*N*-di-*n*-propyl substitution binds better into the CRFR1 pocket.

3. Conclusion

Ten new thiazolo[4,5-*d*]pyrimidine derivatives were synthesized and pharmacologically assessed for CRFR1 antagonist activity. Compound **8c** was the most promising candidate and was able to cause more than

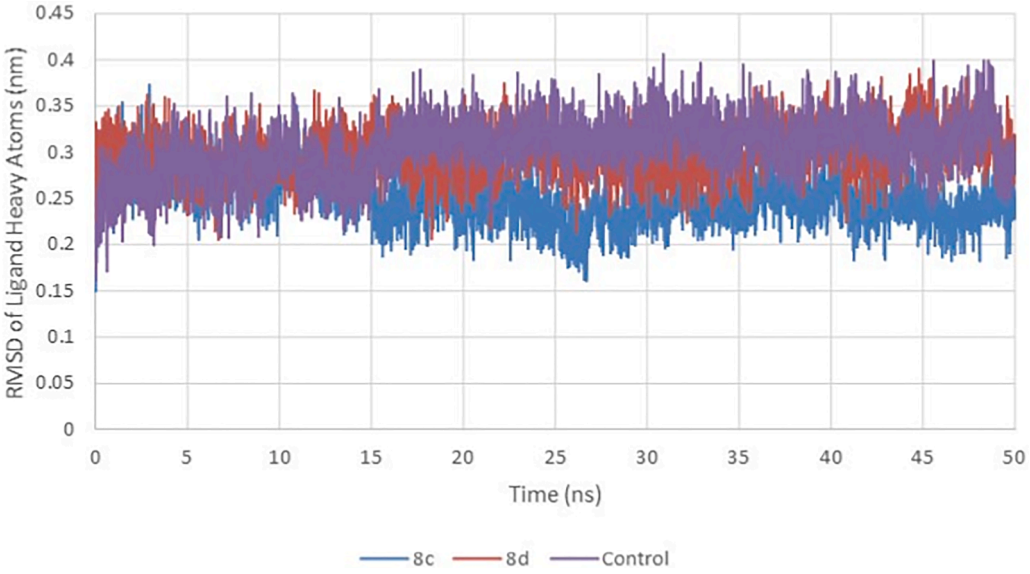

Fig. 9. Plot of the RMSD of the ligands heavy atoms in the allosteric site of CRFR1 of both co-crystalized ligand, compounds **8c**, **8d** and control.

Table 4
MM-PBSA calculations for CRFR1 complexes with co-crystalized ligand (control) and **8c**.

	Energies (kJ/mol)	
	Control	**8c**
van der Waal energy	−226.457 ± 9.611	−276.721 ± 10.708
Electrostatic energy	−24.824 ± 2.873	−36.149 ± 5.682
Polar solvation energy	97.283 ± 8.519	133.675 ± 11.575
SASA energy	−21.915 ± 0.802	−23.371 ± 0.808
Binding energy	−175.913 ± 12.113	−202.565 ± 13.976

50% Inhibition of [^{125}I]-Tyr^{0}-sauvagine specific binding. In addition, **8c** showed good binding affinity compared to antalarmin and was able to inhibit CRF induced cAMP accumulation in a dose response manner exhibiting an IC_{50} of 2.15 μM. Compound **8c** was also found to have similar binding mode compared to co-crystalized ligand CP-376395 based on docking studies and the complex of **8c** with CRFR1 was found to be stable as suggested by the molecular dynamics study.

4. Experimental

4.1. Chemistry

4.1.1. General methods

Solvents, reagents and starting materials were obtained from Merck (Darmstadt, Germany), Acros Organics (New Jersy, USA) and Sigma Aldrich (Missori, USA). Reactions were monitored using thin-layer chromatography (TLC) using aluminum sheets pre coated with silica gel (Kieselgel, F254, pore size 60 Å, Merck, Darmstadt, Germany) and observed under a UV lamp (short-wavelength, 254 nm). Silica gel (pore size 60 Å, 230–400 mesh particle size, Merck, Darmstadt, Germany) was used for column chromatography. Stuart melting point apparatus (Stuart Scientific, Redhill, UK) was used for the determination of melting points. Infra-red (IR) spectra were obtained using an FT-IR spectrometer using KBr discs (Perkin Elmer, Waltham, Massachusetts). NMR spectra were obtained using Varian NMR spectrometer (Varian Inc., Palo Alto, California) operating at 300 MHz for ^{1}H NMR and 75 MHz for ^{13}C NMR at Dr. Ahmed Farag Laboratory, Faculty of Science, Cairo University or using Bruker NMR spectrometer (Bruker

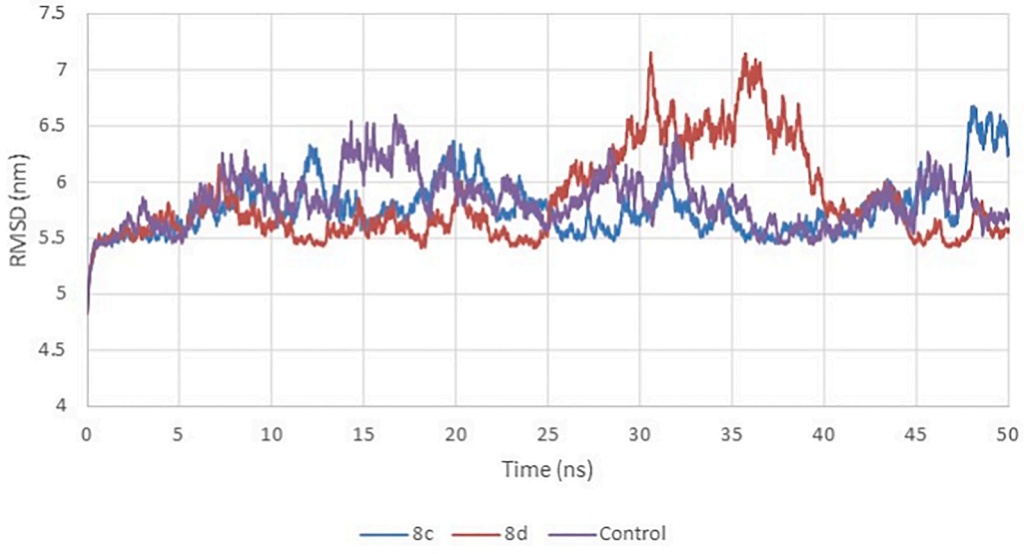

Fig. 10. Plot of protein RMSD relative to crystal structure of **8c**, **8d** and co-crystalized ligand.

Biospin GmbH, Rheinstetten, Germany), operating at 400 MHz for ^{1}HNMR and 100 MHz for ^{13}C at Center for Drug Discovery Research and Development, Faculty of Pharmacy Ain Shams University. Chemical shifts are expressed in δ values (ppm) relative to TMS using DMSO-d_6 or $CDCl_3$ as solvents. Electron impact mass spectrometry (EI-MS) spectra were obtained at the Regional Center for Mycology and Biotechnology, Al-Azhar University using Thermo Scientific ISQ LT mass spectrometer (Thermo Fisher Scientific Inc., Waltham, Massachusetts). Electrospray ionization mass (ESI-MS) spectra were collected at the Faculty of Pharmacy, Helwan University on Thermo Scientific mass spectrometer LC-MS (Thermo Fisher Scientific Inc., Waltham, Massachusetts). Elemental analyses were done on a Thermo Scientific Flash 2000 elemental analyzer (Thermo Fisher Scientific Inc., Waltham, Massachusetts) at Regional Center for Mycology and Biotechnology, Al-Azhar University. Compounds **1**, **2**, **3**, **4**, **6** and **7** were prepared as reported earlier [36].

*4.1.2. Synthesis of 7-(Dialkylamino)-3-(2,4-dimethoxyphenyl)-5-methylthiazolo[4,5-d]pyrimidine-2(3H)-thione (**5a-e**):*

General procedure: A mixture of compound **4 (**1 g, 2.83 mmol) was reacted with the appropriate dialkyl amine (5.66 mmol) in absolute ethanol (15 ml) with gentle heating (70℃) for 3–6 h., the reaction mixture was allowed to cool down then poured onto ice water and stirred for 30 min. The obtained precipitate was filtered and recrystallized from absolute ethanol or the aqueous solution was extracted with ethyl acetate then the organic extracts were collected, dried over anhydrous sodium sulfate and concentrated under reduced pressure.

*4.1.2.1. 3-(2,4-Dimethoxyphenyl)-5-methyl-7-(propylamino)thiazolo[4,5-d]pyrimidine-2(3H)-thione (**5a**):*. Reflux time: 3 h. Light yellow powder; **yield** 85%; **m.p.** 129℃; IR (KBr) ν cm^{-1}: 3383 (NH); ^{1}H NMR (400 MHz, DMSO-d_6) δ ppm: 0.45 – 1.27 (m, 5H, C_2H_5), 1.58 (s, 2H, CH_2), 2.27 (s, 3H, CH_3), 3.68 (s, 3H, OCH_3), 3.84 (s, 3H, OCH_3), 6.65 (s, 1H, aromatic), 6.76 (s, 1H, aromatic), 7.16 (s, 1H, aromatic), 7.82 (s, 1H, NH); ^{13}C NMR (100 MHz, DMSO-d_6) δ ppm: 11.39 (CH_3), 22.08 (CH_2), 25.57 (CH_3), 42.16 (CH_2), 55.50 (OCH_3), 55.92 (OCH_3), 96.84, 99.66, 105.53, 117.32, 130.61, 154.64, 155.69, 158.58, 161.33, 165.46 (10C, aromatic), 189.58 (C_2, thioxo); **MS** (*m/z*, %): 376.05 (M^+, 8.76), 40.15 (Bp, 100); **Anal.** Calcd. for $C_{17}H_{20}N_4O_2S_2$ 376.49: C, 54.23; H, 5.35; N, 14.88; S, 17.03, Found: C, 54.26; H, 5.32; N, 14.89; S, 17.02.

*4.1.2.2. 7-(Diethylamino)-3-(2,4-dimethoxyphenyl)-5-methylthiazolo[4,5-d]pyrimidine-2(3H)-thione (**5b**):*. Reflux time: 3 h. Light buff powder; **yield** 85%; **m.p.** 141℃; IR (KBr) ν cm^{-1}: No significant peaks; ^{1}H NMR (400 MHz, DMSO-d_6) δ ppm: δ 1.22 (t, J = 7.00 Hz, 6H, $2CH_3$), 2.28 (s, 3H CH_3), 3.60 (h, J = 7.30 Hz, 4H, $2CH_2$), 3.70 (s, 3H,OCH_3), 3.86 (s, 3H,OCH_3), 6.67 (dd, J = 8.9, 2.5 Hz, 1H aromatic), 6.78 (d, J = 2.5 Hz, 1H aromatic), 7.17 (d, J = 8.7 Hz, 1H aromatic); ^{13}C NMR (75 MHz, DMSO-d_6) δ ppm: 13.91 ($2CH_3$), 25.46 (CH_3), 42.82 ($2CH_2$), 55.59 (OCH_3), 56.06 (OCH_3), 99.88, 105.74, 117.52, 120.98, 130.61, 154.30, 155.81, 161.45, 164.73, 164.84 (10C, aromatic), 188.87 (C_2, thioxo); MS (EI) *m/z* (%): 390.54 (M^+, 18.62), 57.03 (Bp, 100); **Anal.** Calcd. for $C_{18}H_{22}N_4O_2S_2$ 390.54: C, 55.36; H, 5.68; N, 14.35; S, 16.42, Found: C, 55.38; H, 5.65; N, 14.39; S, 16.43.

*4.1.2.3. 3-(2,4-Dimethoxyphenyl)-7-(dipropylamino)-5-methylthiazolo[4,5-d]pyrimidine-2(3H)-thione (**5c**):*. Reflux time: 3.5 h. Greenish yellow crystals, **yield** (81%) **m.p.** 137℃; IR (KBr) ν cm^{-1}: No significant peaks; ^{1}H NMR (400 MHz, $CDCl_3$) δ ppm: 1.00 (t, J = 7.40 Hz, 6H, $2CH_3$), 1.67 – 1.78 (sixtet, 4H , 2 CH_2), 2.40 (s, 3H , CH_3), 3.54 (t, 4H, 2 CH_2), 3.77 (s, 3H,OCH_3), 3.89 (s, 3H, OCH_3), 6.65 – 6.67 (m, 1H, aromatic), 6.68 (d, J = 2.6 Hz, 1H,aromatic), 7.16 (d, J = 9.3 Hz, 1H, aromatic); ^{13}C NMR (100 MHz, DMSO-d_6) δ ppm: 11.34 ($2CH_3$), 22.05 ($2CH_2$), 25.99 (CH_3), 50.68 ($2CH_2$), 55.99 (OCH_3), 56.42 (OCH_3), 100.14, 106.08, 117.84, 131.06, 155.00, 156.15, 160.24, 161.83, 165.16, 167.96 (10C, aromatic), 189.15 (C_2, thioxo); MS (EI) *m/z* (%): 418.14 (M^+, 18.62), 274.15 (Bp, 100); **Anal.** Calcd. for $C_{20}H_{26}N_4O_2S_2$ 418.15: C, 57.39; H, 6.26; N, 13.39; S, 15.32, Found: C, 57.43; H, 6.23; N, 13.41; S, 15.31.

*4.1.2.4. 7-(Dibutylamino)-3-(2,4-dimethoxyphenyl)-5-methylthiazolo[4,5-d]pyrimidine-2(3H)-thione (**5d**):*. Reflux time: 6 h. Buff powder, **yield** 83%; **m.p.** 128℃; IR (KBr) ν cm^{-1}: No significant peaks; ^{1}H NMR (400 MHz, DMSO-d_6) δ ppm: 0.95 (t, J = 7.3 Hz, 6H, $2CH_3$), 1.36 (sixtet, J = 7.2 Hz, 4H, $2CH_2$), 1.61 (p, J = 7.5 Hz, 4H $2CH_2$), 2.26 (s, 3H,CH_3), 3.55 (d, J = 7.6 Hz, 4H, $2CH_2$), 3.70 (s, 3H,OCH_3), 3.86 (s, 3H,OCH_3), 6.67 (dd, J = 8.7, 2.3 Hz, 1H, aromatic), 6.78 (d, J = 2.2 Hz, 1H, aromatic), 7.17 (d, J = 8.6 Hz, 1H, aromatic); ^{13}C NMR (100 MHz, DMSO-d_6) δ ppm: 14.24 ($2CH_3$), 19.89 ($2CH_2$), 25.94 (CH_3), 30.88 ($2CH_2$), 48.72 ($2CH_2$), 55.99 (OCH_3), 56.41 (OCH_3), 95.67, 100.13, 106.08, 117.83, 131.05, 154.92, 156.13, 160.23, 161.83, 165.13 (10C, aromatic), 189.11 (C_2, thioxo); MS (EI) *m/z* (%): 446.32 (M^+, 5.62), 57.02 (Bp, 100); **Anal.** Calcd. for $C_{22}H_{30}N_4O_2S_2$ 446.63: C, 59.16; H, 6.77; N, 12.54; S, 14.36. Found: C, 59.2; H, 6.75; N, 12.57; S, 14.39.

*4.1.2.5. 7-(Butyl(ethyl)amino)-3-(2,4-dimethoxyphenyl)-5-methylthiazolo[4,5-d]pyrimidine-2(3H)-thione (**5e**):*. Reflux time: 5 h. Yellowish brown crystals; **yield** 62%; **m.p.** 109 ℃; IR (KBr) ν cm^{-1}: no significant peaks; ^{1}H NMR (400 MHz, $CDCl_3$) δ ppm: 1.01 (t, J = 7.3 Hz, 3H, CH_3), 1.28 (t, J = 7.0 Hz, 3H, CH_3), 1.43 (h, J = 7.4 Hz, 2H, CH_2), 1.69 (p, J = 7.6 Hz, 2H, CH_2), 2.39 (s, 3H, CH_3), 3.55 (t, J = 6. 8 Hz, 2H, CH_2), 3.66 (qd, J = 7.1, 2.7 Hz, 2H, CH_2), 3.77 (s, 3H, OCH_3), 3.89 (s, 3H, OCH_3), 6.65 – 6.69 (m, 2H, aromatic), 7.17 (d, J = 9.3 Hz, 1H, aromatic); ^{13}C NMR (100 MHz, DMSO-d_6) δ ppm: 14.17 (CH_3), 14.23 (CH_3), 19.93 (CH_2), 25.95 (CH_3), 31.05 (CH_2), 43.73 (CH_2-N), 48.22 (CH_2-N), 55.98 (OCH_3), 56.40 (OCH_3), 95.67, 100.13, 106.05, 117.85, 131.02, 154.78, 156.15, 160.23, 161.83, 165.20 (10C, aromatic), 189.17 (C_2, thioxo); MS (EI) *m/z* (%): 418.14 (M^+, 11.63), 98.44 (Bp, 100); **Anal.** Calcd. for $C_{20}H_{26}N_4O_2S_2$ 418.57: C, 57.39; H, 6.26; N, 13.39; S, 15.32, Found: C, 57.42; H, 6.24; N, 13.42; S, 15.36.

*4.1.3. 3-(2,4-Dimethoxyphenyl)-7-(dialkylamino)-5-methylthiazolo[4,5-d]pyrimidin-2(3H)-one (**8a-e**):*

General procedure: A mixture of compound **7 (**1 g, 2.96 mmol) and the appropriate dialkyl amine (5.92 mmol) in absolute ethanol (15 ml) using the same procedures described for **5a-e.**

*4.1.3.1. 3-(2,4-Dimethoxyphenyl)-5-methyl-7-(propylamino)thiazolo[4,5-d]pyrimidin-2(3H)-one (**8a**):*. Reflux time: 3 h. Light yellow powder; yield 85%; m.p. 124℃; ^{1}H NMR (400 MHz, DMSO-d_6) δ ppm: 0.76 – 0.99 (m, 5H, overlapped CH_2 and CH_3), 1.51 – 1.66 (m, 2H, CH_2), 2.27 (s, 3H, CH_3), 3.69 (s, 3H, OCH_3), 3.85 (s, 3H, OCH_3), 6.66 (dd, J = 8.7, 2.5 Hz, 1H, aromatic), 6.77 (d, J = 2.5 Hz, 1H, aromatic), 7.16 (d, J = 8.6 Hz, 1H, aromatic), 7.82 (s, 1H, NH); ^{13}C NMR (100 MHz, DMSO-d_6) δ ppm: 11.39 (CH_3), 22.07 (CH_2), 25.58 (CH_3), 42.15 (CH_2), 55.51(OCH_3), 55.93 (OCH_3), 89.20, 99.66, 105.54, 117.30, 130.61, 131.11, 151.88, 154.77, 155.68, 161.32 (10C, aromatic), 165.45 (C_2, C═O); MS (EI) *m/z* (%): 360.19 (M^+, 9.39), 62.90 (Bp, 100); **Anal.** Calcd. for $C_{17}H_{20}N_4O_3S$ 360.43: C, 56.65; H, 5.59; N, 15.54; S, 8.89. Found: C, 56.67; H, 5.57; N, 15.53; S, 8.87.

*4.1.3.2. 7-(Diethylamino)-3-(2,4-dimethoxyphenyl)-5-methylthiazolo[4,5-d]pyrimidin-2(3H)-one (**8b**):*. Reflux time: 3 h. Light buff powder; yield 87%; m.p. 151℃; IR (KBr) ν cm^{-1}: 1702 (C_2, (C═O)); ^{1}H NMR (400 MHz, DMSO-d_6) δ ppm: 1.20 (t, J = 6.9 Hz, 6H, $2CH_3$), 2.24 (s, 3H, CH_3), 3.59 (sixtet, J = 7.1 Hz, 4H, $2CH_2$), 3.72 (s, 3H, OCH_3), 3.84 (s, 3H, OCH_3), 6.64 (dd, J = 8.6, 2.7 Hz, 1H, aromatic), 6.75 (d, J = 2.6 Hz, 1H, aromatic), 7.23 (d, J = 8.6 Hz, 1H, aromatic); ^{13}C NMR (100 MHz, DMSO-d_6) δ ppm: 14.11 ($2CH_3$), 25.57 ($2CH_2$), 42.56 (CH_3), 55.53 (OCH_3), 55.89 (OCH_3), 89.12, 99.41, 105.31, 115.38, 130.75, 154.69,

156.01, 156.14, 161.24, 163.62 (10C, aromatic), 167.40 (C_2, C═O); MS (EI) *m/z* (%): 373.98 (M^+, 9.13), 57.05 (Bp, 100); **Anal.** Calcd for $C_{18}H_{22}N_4O_3S$ 374.14: C, 57.74; H, 5.92; N, 14.96; S, 8.56. Found: C, 57.76; H, 5.90; N, 14.99; S, 8.59.

*4.1.3.3. 3-(2,4-Dimethoxyphenyl)-7-(dipropylamino)-5-methylthiazolo [4,5-d]pyrimidin-2(3H)-one (**8c**):*. Reflux time: 3.5 h. Light yellow powder; yield 82%; m.p. 133℃; IR (KBr) ν cm^{-1}: 1695 (C_2 C═O); ^{1}H NMR (400 MHz, DMSO-d_6) δ ppm: 0.91 (d, J = 7.3 Hz, 6H, $2CH_3$), 1.63 (m, J = 7.5 Hz, 4H, $2CH_3$), 2.23 (s, 3H, CH_3), 3.49 (td, J = 7.2, 2.5 Hz, 4H, $2CH_2$), 3.72 (s, 3H, OCH_3), 3.84 (s, 3H, OCH_3), 6.63 (dd, J = 8.7, 2.6 Hz, 1H, aromatic), 6.75 (d, J = 2.6 Hz, 1H, aromatic), 7.22 (d, J = 8.6 Hz, 1H, aromatic). ^{13}C NMR (100 MHz, DMSO-d_6) δ ppm: 10.82 (CH_3), 21.77 (CH_2), 25.56 (CH_3), 50.08 (CH_2), 55.53 (OCH_3), 55.89 (OCH_3), 89.18, 99.41, 105.32, 115.36, 130.76, 155.01, 156.00, 156.16, 161.23, 163.49 (10C, aromatic), 167.32(C_2, C═O); MS (EI) *m/z* (%): 402.17 (M^+, 8.03), 57.63 (Bp, 100); **Anal.** Calcd for $C_{20}H_{26}N_4O_3S$, 402.17: C, 59.68; H, 6.51; N, 13.92; S, 7.96. Found: C, 59.65; H, 6.53; N, 13.90; S, 7.93.

*4.1.3.4. 7-(Dibutylamino)-3-(2,4-dimethoxyphenyl)-5-methylthiazolo [4,5-d]pyrimidin-2(3H)-one (**8d**):*. Reflux time: 6 h. Light buff powder; **yield** 70%; **m.p.** 106℃; ^{1}H NMR (400 MHz, DMSO-d_6) δ ppm: 0.94 (t, J = 7.4 Hz, 6H, $2CH_3$), 1.34 (h, J = 7.3 Hz, 4H, $2CH_2$), 1.59 (p, J = 7.5 Hz, 4H, $2CH_2$), 2.22 (s, 3H, CH_3), 3.48 – 3.60 (m, 4H, $2CH_2$), 3.72 (s, 3H, OCH_3), 3.84 (s, 3H, OCH_3), 6.63 (dd, J = 8.6, 2.6 Hz, 1H, aromatic), 6.75 (d, J = 2.6 Hz, 1H, aromatic), 7.22 (d, J = 8.7 Hz, 1H, aromatic); ^{13}C NMR (100 MHz, DMSO-d_6) δ ppm: 14.26 ($2CH_3$), 19.86 ($2CH_2$), 26.01 (CH3), 31.13 ($2CH_2$), 48.59 ($2CH_2$), 56.02 (OCH_3), 56.38 (OCH_3), 98.31, 99.96, 105.81, 115.82, 130.99, 131.25, 156.48, 157.96, 161.72, 162.26 (10C, aromatic), 163.97 (C_2, C═O); MS (EI) *m/z* (%): 429.88 (M^+, 2.90), 186.99 (Bp, 100); **Anal.** Calcd for $C_{22}H_{30}N_4O_3S$, 430.17: C, 61.37; H, 7.02; N, 13.01; S, 7.45. Found: C, 61.39; H, 7.04; N, 12.98; S, 7.47.

*4.1.3.5. 7-(Butyl(ethyl)amino)-3-(2,4-dimethoxyphenyl)-5-methylthiazolo [4,5-d]pyrimidin-2(3H)-one (**8e**):*. Reflux time: 5 h. Brownish yellow powder; **yield** 65%; **m.p.** 125℃; IR (KBr) ν cm^{-1}: 1693 (C_2, C═O); ^{1}H NMR (400 MHz, DMSO-d_6) δ ppm: 0.74 – 1.69 (m, 10*H*, aliphatic), 2.22 (s, 3H, CH_3), 2.84 (d, 2H, CH_2) 3.57 (s, 2H, CH_2), 3.71 (s, 3H, OCH_3), 3.83 (s, 3H, OCH_3), 6.62 (d, J = 8.9 Hz, 1H, aromatic), 6.74 (s, 1H, aromatic), 7.35 (d, J = 8.8 Hz, 1H, aromatic); ^{13}C NMR (100 MHz, DMSO-d_6) δ ppm: 14.15 (CH_3), 14.24 (CH_3), 19.92 (CH_2), 25.96 (CH_2), 31.03 (CH_3), 43.73 (CH_2), 48.21 (CH_2), 55.99 (OCH_3), 56.41 (OCH_3), 95.66, 100.13, 106.07, 117.83, 131.04, 154.78, 156.14, 160.21, 161.83, 165.21 (10C, aromatic), 189.17 (*C*2, C═O); MS (EI) *m/z* (%): 402.79 (M+, 4.30), 57.98 (Bp, 100); **Anal.** Calcd for $C_{20}H_{26}N_4O_3S$, 402.17: C, 59.68; H, 6.51; N, 13.92; S, 7.96. Found: C, 59.71; H, 6.48; N, 13.89; S, 7.93.

4.2. Biological evaluation

4.2.1. Iodinating Tyr^0-SVG

The radioiodination of Tyr^0-Sauvagine (Tyr^0-SVG) was performed using Pre-Coated Iodination Tubes. In specific, 50 μL of Tris Iodination Buffer (25 mM Tris•HCl, and 0.4 M NaCl, pH 7.4) were added into Pre-Coated Iodination Tubes (Pierce, Cat. No 28601). Subsequently 20 μL containing 1 mCi Na^{125}I (Perkin Elmer, Cat. No NEZ033A) were added. After 6 min incubation at room temperature, the mixture was added into a low retention tube (Kisker, Cat. No G016) containing 7 μg of Tyr^0-SVG (in 1.5 μL of Tris Iodination Buffer). After 10 min incubation at room temperature, 20 μL of scavenging buffer (10 mg tyrosine/ml in Tris Iodination Buffer) was added into the mixture and the incubation continued for 5 min at room temperature. After adding 1 ml of elution buffer (0.1% TFA), the radiodinated species were loaded onto a Sep-Pak C-18 cartridge (Waters WAT051910) and separated by sequential elution with solutions (1 ml each) containing 5, 10, 20, 30, 35, 40, 50, 60, 80% acetonitrile in water and 0.1% TFA. Fractions of 0.5 ml were collected and their radioactivity was determined. Subsequently, 3.5 μL mercaptoethanol and 10 μL 20% BSA were added to three fractions, eluted with 35% and 40% acetonitrile, containing radioiodinated Tyr^0-sauvagine.

4.2.2. CRFR1 binding study

Binding studies was performed according to our reported procedure [37] in membrane homogenates from human embryonic kidney cells (HEK 293) stably expressing CRFR1 and using [^{125}I]-Tyr^0-sauvagine as radioligand. Membrane homogenates were prepared according to the method of Spyridaki et al [35]. CRFR1 -expressing HEK 293 cells, grown in DMEM/F12 (1:1) containing 3.15 g/L glucose, 10% bovine calf serum and 300 μg/ml of the antibiotic, Geneticin at 37 °C and 5% CO_2, were washed with phosphate-buffered saline (PBS) (4.3 mM Na_2HPO_4.7 H_20, 1.4 mM KH_2PO_4, 137 mM NaCl, 2.7 mM KCl, pH 7.2–7.3 at R.T). Then the cells were briefly treated with PBS containing 2 mM EDTA (PBS/EDTA), and then dissociated in PBS/EDTA. Cells suspensions were centrifuged at 1000 × g for 5 min at room temperature, and the pellets were homogenized in 1.5 ml of buffer H (20 mM HEPES, containing 10 mM $MgCl_2$, 2 mM EGTA, 0.2 mg/ml bacitracin and 0.93 μg/ml aprotinin pH 7.2 at 4 °C) using a Janke & Kunkel IKA Ultra Turrax T25 homogenizer, at setting ~ 20, for 10–15 *sec*, at 4 °C. The homogenates were centrifuged at 16000 × g, for 10 min, at 4 °C. The membrane pellets were re-suspended by homogenization, as described above, in 1 ml buffer B (buffer H containing 0.1% BSA, pH 7.2 at 20 °C). The membrane suspensions were then diluted in buffer B and aliquots of suspensions (50 μL) were added into tubes containing buffer B and 20000–30000 cpm [^{125}I]-Tyr^{0}sauvagine without or with the new test compounds at the single concentration of 500 nM (screening experiments) or with increasing concentrations of HR compounds or antalarmin (heterologous competition binding experiments) or increasing concentrations of Tyr^{0}sauvagine (homologous competition binding experiments) in a final volume of 0.2 ml. The mixtures were incubated at 20-21° C for 120 min and then were filtered through Whatman 934AH filters, presoaked for 1 h in 0.3% polyethylene imine at 4° C. The filters were washed 3 times with 0.5 ml of ice-cold PBS, pH 7.1 containing 0.01% Triton X-100 and assessed for radioactivity in a gamma counter. The amount of membranes used were adjusted to ensure that the specific binding is always equal to or less than 10% of the total concentration of the added radioligand. Specific [^{125}I]-Tyr^0-sauvagine binding was defined as total binding less nonspecific binding in the presence of excess of cold ligand (1 μM antalarmin or 0.3 μM sauvagine). Data for competition binding was analyzed by nonlinear regression analysis, using Prism 4.0 (GraphPad Software, San Diego, CA). IC_{50} values were obtained by fitting the data from competition studies to a one-site competition model. The binding affinities for HR compounds and antalarmin ($logK_i$ values) and for ^{125}I-Tyr^0-sauvagine ($logK_D$ values) were determined from heterologous and homologous competition data, respectively, as described previously using Prism 4.0 [37].

4.2.3. FRET assays for detection of cAMP

FRET assays reported here used a new C4 clone of HEK293 cells created by O.G. Cherpurny. These HEK293-C4 cells were doubly stably transfected with the human CRFR1 and also the cAMP biosensor H188. The methods of transfection, clonal selection, and FRET analysis in a 96-well format were identical to those reported in greater detail by Chepurny and colleagues for assays monitoring glucagon action at the human glucagon receptor [38]. Briefly, suspensions of HEK293-C4 cells were prepared in a standard extracellular saline (SES) solution containing (in mM): 138 NaCl, 5.6 KCl, 2.6 CaCl2, 1.2 MgCl2, 11.1 glucose, 10 Hepes (295 mosmol, pH 7.4) supplemented with 0.1% BSA. Individual wells of a 96-well clear-bottom assay plate (Costar 3904, Corning, NY) received 200 μL/well cell suspension so that real-time kinetic assays

of FRET could be performed using a Flexstation 3 microplate reader (Molecular Devices, Sunnyvale, CA). Test solutions dissolved in SES were placed in V-bottom 96-well plates (Greiner Bio-One, Monroe, NC) so that an automated pipetting procedure could be used to transfer 50 μL of each test solution to each well of the assay plate containing cells. To monitor binding of cAMP to H188, the excitation light was delivered at 435/9 nm, and the emitted light was detected at 485/15 nm (mTurquoise2Δ FRET donor) or 535/15 nm (cp173 Venus-Venus FRET acceptor). An increase of the 485/535 nm FRET ratio signifies an increase of cAMP concentration [39]. FRET ratio values were normalized using baseline subtraction so that a y axis value of 0 corresponds to the initial baseline FRET ratio, whereas a value of 100 corresponds to a 100% increase (i.e. doubling) of the FRET ratio. The time course of the ΔFRET ratio was plotted after exporting data to Origin 8.0 (OriginLab, Northampton, MA). Origin 8.0 was also used for nonlinear regression analysis to quantify dose–response relationships.

4.3. Molecular modelling studies

4.3.1. Molecular Docking

The proposed binding mode of tested compounds with Corticotrophin releasing factor receptor (CRFR1) was studied using Autodock Vina [40] Compounds were built and prepared as reported earlier [41] Crystal structure of CRFR1 (PDB ID:4K5Y) was used after adding hydrogens, removing waters, and adding Gasteiger charges. Prepared and co-crystalized ligands were docked in a grid box in the allosteric site (25*25*25 $Å^3$, centered on co-crystalized ligand) using exhaustiveness of 16. For each ligand, the top 9 binding poses were ranked according to their binding affinities and the predicted binding interactions were analyzed. The pose with the best binding affinity and binding mood similar to co-crystalized ligand was reported. 3D images were prepared using PyMOL software.

4.3.2. Molecular dynamics

Docking poses were used as initial coordinates for molecular dynamics simulation. Missing loop (221–223) of CRFR1 was build using SWISS-MODEL [42] and was filled with YST sequence. Preparation of protein and ligands and used parameters were done according to methods reported earlier [43]. In summary, CHARMM36 all-atom force field [44] was used for protein parameterization while ligands parameters were obtained from SwissParam [45] Complexes were built, boxed in dodecahedron box, solvated with TIP3P water [46] and neutralized with Na^+ or Cl^- ions as needed. All molecular dynamics simulations were done using GROMACS 2020.3 [47] Initially, complexes were minimized using steepest descent algorithm and maximum force was set to less than 1000 kJ mol^{-1} nm^{-1} then systems were equilibrated using 100 ps of NVT followed by NPT ensembles. V-rescale thermostat [48] was used to control temperature at 300 ^oK while Parrinello-Rahman barostat [49] was used to control pressure. Particle mesh Ewald (PME) method [50] was used for calculation of long-range electrostatics. Timestep of 2 fs was used for all simulations and Van der Waals cut-off distance (rvdw) of 1.2 nm was used. MM-PBSA calculation was done using g_mmpbsa tool [51].

Declaration of Competing Interest

The authors declare that they have no known competing financial interests or personal relationships that could have appeared to influence the work reported in this paper.

Acknowledgements

This work was partially funded by NIH grant funding (NIH R01 DK069575) received by Professor G. Holz.

Appendix A. Supplementary data

Supplementary data to this article can be found online at https://doi.org/10.1016/j.bioorg.2021.105079.

References

[1] G.N. Smagin, A.J. Dunn, The role of CRF receptor subtypes in stress-induced behavioural responses, Eur. J. Pharmacol. 405 (2000) 199–206, https://doi.org/10.1016/S0014-2999(00)00553-7.
[2] W. Vale, J. Spiess, C. Rivier, J. Rivier, Characterization of a 41-residue ovine hypothalamic peptide that stimulates secretion of corticotropin and β-endorphin, Obstet. Gynecol. Surv. 37 (1982) 334, https://doi.org/10.1097/00006254-198205000-00013.
[3] K. Van Pett, V. Viau, J.C. Bittencourt, R.K.W. Chan, H.Y. Li, C. Arias, G.S. Prins, M. Perrin, W. Vale, P.E. Sawchenko, Distribution of mRNAs encoding CRF receptors in brain and pituitary of rat and mouse, J. Comp. Neurol. 428 (2000) 191–212, https://doi.org/10.1002/1096-9861(20001211)428:2<191::AID-CNE1>3.0.CO;2-U.
[4] F. Holsboer, M. Ising, Central CRH system in depression and anxiety - Evidence from clinical studies with CRH1 receptor antagonists, Eur. J. Pharmacol. 583 (2008) 350–357, https://doi.org/10.1016/j.ejphar.2007.12.032.
[5] A.V. Kaluev, D.J. Nutt, On the role of GABA in anxiety and depression, Eksp. i Klin. Farmakol. 67 (2004) 71–76. https://doi.org/10.30906/0869-2092-2004-67-4-71-76.
[6] G. Aguilera, M. Flores, P. Carvallo, J.P. Harwood, M. Millan, K.J. Catt, M. Flores, P. Carvallo, J.P. Harwood, M. Millan, K.J. Catt, Receptors for Corticotropin-Releasing Factor, in: Corticotropin-Releasing Factor Basic Clin. Stud. a Neuropept, 1st ed.,, CRC Press, 2018, pp. 153–174, https://doi.org/10.1201/9781351070935-11.
[7] C. Rivier, M. Smith, W. Vale, Regulation of adrenocorticotropic hormone (ACTH) secretion by corticotropin-releasing factor (CRF), in: Corticotropin-Releasing Factor Basic Clin. Stud. a Neuropept, 1st editio,, CRC Press, 2018, pp. 175–189, https://doi.org/10.1201/9781351070935.
[8] J.A. Majzoub, Corticotropin-releasing hormone physiology, Eur. J. Endocrinol. Suppl. 155 (2006) S71–S76, https://doi.org/10.1530/eje.1.02247.
[9] C. Chen, Recent Advances in Small Molecule Antagonists of the Corticotropin-Releasing Factor Type-1 Receptor-Focus on Pharmacology and Pharmacokinetics, Curr. Med. Chem. 13 (2006) 1261–1282, https://doi.org/10.2174/092986706776873014.
[10] É.M. Fekete, E.P. Zorrilla, Physiology, pharmacology, and therapeutic relevance of urocortins in mammals: Ancient CRF paralogs, Front. Neuroendocrinol. 28 (2007) 1–27, https://doi.org/10.1016/j.yfrne.2006.09.002.
[11] T.L. Bale, W.W. Vale, CRF and CRF Receptors : Role in Stress Responsivity and Other Behaviors, Annu. Rev. Pharmacol. Toxicol. 44 (2004) 525–557, https://doi.org/10.1146/annurev.pharmtox.44.101802.121410.
[12] E.P. Zorrilla, G.F. Koob, Progress in corticotropin-releasing factor-1 antagonist development, Drug Discov. Today. 15 (2010) 371–383, https://doi.org/10.1016/j.drudis.2010.02.011.
[13] M. Arai, I.Q. Assil, A.B. Abou-Samra, Characterization of three corticotropin-releasing factor receptors in catfish: A novel third receptor is predominantly expressed in pituitary and urophysis, Endocrinology. 142 (2001) 446–454, https://doi.org/10.1210/endo.142.1.7879.
[14] P. Timpl, R. Spanagel, I. Sillaber, A. Kresse, J.M.H.M. Reul, G.K. Stalla, V. Blanquet, T. Steckler, F. Holsboer, W. Wurst, Impaired stress response and reduced anxiety in mice lacking a functional corticotropin-releasing hormone receptor 1, Nat. Genet. 19 (1998) 162–166, https://doi.org/10.1038/520.
[15] G.W. Smith, J.M. Aubry, F. Dellu, A. Contarino, L.M. Bilezikjian, L.H. Gold, R. Chen, Y. Marchuk, C. Hauser, C.A. Bentley, P.E. Sawchenko, G.F. Koob, W. Vale, K.F. Lee, Corticotropin releasing factor receptor 1-deficient mice display decreased anxiety, impaired stress response, and aberrant neuroendocrine development, Neuron. 20 (1998) 1093–1102.
[16] M.P. Stenzel-Poore, S.C. Heinrichs, S. Rivest, G.F. Koob, W.W. Vale, Overproduction of corticotropin-releasing factor in transgenic mice: a genetic model of anxiogenic behavior, J. Neurosci. 14 (1994) 2579–2584.
[17] S.C. Heinrichs, J. Lapsansky, T.W. Lovenberg, E.B. De Souza, D.T. Chalmers, Corticotropin-releasing factor CRF1, but not CRF2, receptors mediate anxiogenic-like behavior, Regul. Pept. 71 (1997) 15–21.
[18] G. Liebsch, R. Landgraf, R. Gerstberger, J.C. Probst, C.T. Wotjak, M. Engelmann, F. Holsboer, A. Montkowski, Chronic infusion of a CRH1 receptor antisense oligodeoxynucleotide into the central nucleus of the amygdala reduced anxiety-related behavior in socially defeated rats, Regul. Pept. 59 (1995) 229–239.
[19] G. Liebsch, R. Landgraf, M. Engelmann, P. Lörscher, F. Holsboer, Differential behavioural effects of chronic infusion of CRH 1 and CRH 2 receptor antisense oligonucleotides into the rat brain, J. Psychiatr. Res. 33 (1999) 153–163.
[20] T. Skutella, J.C. Probst, U. Renner, F. Holsboer, C. Behl, Corticotropin-releasing hormone receptor (type I) antisense targeting reduces anxiety, Neuroscience. 85 (1998) 795–805.
[21] D.A. Gutman Michael J. Owens, and Charles B. Nemeroff, Corticotropin-releasing factor antagonists as novel psychotherapeutics, Drugs Future. 25 (2000) 923–931. file:///C:/Users/Hosam/AppData/Local/Mendeley Ltd./Mendeley Desktop/Downloaded/Unknown - Unknown - crf antagonists as novel psycothearapeutics.pdf.pdf.

[22] S. Okuyama, S. Chaki, N. Kawashima, Y. Suzuki, S. Ogawa, A. Nakazato, T. Kumagai, T. Okubo, K. Tomisawa, Receptor binding, behavioral, and electrophysiological profiles of nonpeptide corticotropin-releasing factor subtype 1 receptor antagonists CRA1000 and CRA1001, J. Pharmacol. Exp. Ther. 289 (1999) 926–935.

[23] K. Hollenstein, J. Kean, A. Bortolato, R.K.Y.Y. Cheng, A.S. Doré, A. Jazayeri, R. M. Cooke, M. Weir, F.H. Marshall, K. Hollenstein, J. Kean, A. Bortolato, R.K.Y. Y. Cheng, A.S. Dore, M. Weir, F.H. Marshall, Structure of class B GPCR corticotropin-releasing factor receptor 1, Nature. 499 (2013) 438–443, https://doi.org/10.1038/nature12357.

[24] Y. Ye, Q. Liao, J. Wei, Q. Gao, 3D-QSAR study of corticotropin-releasing factor 1 antagonists and pharmacophore-based drug design, Neurochem. Int. 56 (2010) 107–117, https://doi.org/10.1016/j.neuint.2009.09.008.

[25] J.P. Beck, M.A. Curry, R.J. Chorvat, L.W. Fitzgerald, P.J. Gilligan, R. Zaczek, G. L. Trainor, Thiazolo[4,5-d]pyrimidine thiones and -ones as corticotropin-releasing hormone (CRH-R1) receptor antagonists, Bioorganic Med. Chem. Lett. 9 (1999) 1185–1188, https://doi.org/10.1016/S0960-894X(99)00159-6.

[26] B. Kuppast, K. Spyridaki, G. Liapakis, H. Fahmy, Synthesis of substituted pyrimidines as corticotropin releasing factor (CRF) receptor ligands, Eur. J. Med. Chem. 78 (2014) 1–9, https://doi.org/10.1016/j.ejmech.2014.03.040.

[27] M. Teleb, B. Kuppast, K. Spyridaki, G. Liapakis, H. Fahmy, Synthesis of 2-imino and 2-hydrazono thiazolo[4,5-d]pyrimidines as corticotropin releasing factor (CRF) antagonists, Eur. J. Med. Chem. 138 (2017) 900–908, https://doi.org/10.1016/j.ejmech.2017.07.016.

[28] C.L. Graff, G.M. Pollack, Drug transport at the blood-brain barrier and the choroid plexus, Curr. Drug Metab. 5 (2004) 95–108. http://www.ncbi.nlm.nih.gov/pubmed/14965253.

[29] V.A. Levin, Relationship of octanol/water partition coefficient and molecular weight to rat brain capillary permeability, J. Med. Chem. 23 (1980) 682–684, https://doi.org/10.1021/jm00180a022.

[30] H. Pajouhesh, G.R. Lenz, Medicinal chemical properties of successful central nervous system drugs, NeuroRx. 2 (2005) 541–553, https://doi.org/10.1602/neurorx.2.4.541.

[31] C.A. Lipinski, F. Lombardo, B.W. Dominy, P.J. Feeney, Experimental and computational approaches to estimate solubility and permeability in drug discovery and development settings, Adv. Drug Deliv. Rev. 46 (2001) 3–26. http://www.ncbi.nlm.nih.gov/pubmed/11259830.

[32] A. Daina, O. Michielin, V. Zoete, SwissADME: a free web tool to evaluate pharmacokinetics, drug-likeness and medicinal chemistry friendliness of small molecules, Sci. Rep. 7 (2017) 42717, https://doi.org/10.1038/srep42717.

[33] S.H. Mohamed, H.R. Elgiushy, H. Taha, S.F. Hammad, N.A. Abou-Taleb, K.A. M. Abouzid, H. Al-Sawaf, Z. Hassan, An investigative study of antitumor properties of a novel thiazolo[4,5-d]pyrimidine small molecule revealing superior antitumor activity with CDK1 selectivity and potent pro-apoptotic properties, Bioorganic Med. Chem. 28 (2020), 115633, https://doi.org/10.1016/j.bmc.2020.115633.

[34] H. Ulrich, Cyclic Imidoyl Halides, in: Chem. Imidoyl Halides, 1st ed.,, Springer, US, New York, NY, 1968, pp. 193–210, https://doi.org/10.1007/978-1-4684-8947-7_8.

[35] E.W. Bell, Y. Zhang, DockRMSD: An open-source tool for atom mapping and RMSD calculation of symmetric molecules through graph isomorphism, J. Cheminform. 11 (2019), https://doi.org/10.1186/s13321-019-0362-7.

[36] Y.Y. Liao, J.C. Deng, Y.P. Ke, X.L. Zhong, L. Xu, R.Y. Tang, W. Zheng, Isothiocyanation of amines using the Langlois reagent, Chem. Commun. 53 (2017) 6073–6076, https://doi.org/10.1039/c7cc02373a.

[37] K. Spyridaki, M.-T.T. Matsoukas, A. Cordomi, K. Gkountelias, M. Papadokostaki, T. Mavromoustakos, D.E. Logothetis, A.N. Margioris, L. Pardo, G. Liapakis, Structural-functional analysis of the third transmembrane domain of the corticotropin-releasing factor type 1 receptor: role in activation and allosteric antagonism, J. Biol. Chem. 289 (2014) 18966–18977, https://doi.org/10.1074/jbc.M113.544460.

[38] B. Milliken, O. Chepurny, R. Doyle, G. Holz, FRET Reporter Assays for cAMP and Calcium in a 96-well Format Using Genetically Encoded Biosensors Expressed in Living Cells, Bio-Protocol. 10 (2020) 3514–3531. https://doi.org/10.21769/bioprotoc.3641.

[39] J. Klarenbeek, J. Goedhart, A. van Batenburg, D. Groenewald, K. Jalink, Fourth-Generation Epac-Based FRET Sensors for cAMP Feature Exceptional Brightness, Photostability and Dynamic Range: Characterization of Dedicated Sensors for FLIM, for Ratiometry and with High Affinity, PLoS One. 10 (2015) e0122513–e0122513. https://doi.org/10.1371/JOURNAL.PONE.0122513.

[40] O. Trott, A.J. Olson, AutoDock Vina: Improving the speed and accuracy of docking with a new scoring function, efficient optimization, and multithreading, J. Comput. Chem. 31 (2010) 455–461, https://doi.org/https://doi.org/10.1002/jcc.21334.

[41] S.S. Ebada, N.A. Al-Jawabri, F.S. Youssef, A. Albohy, S.M. Aldalaien, A.M. Disi, P. Proksch, In vivo antiulcer activity, phytochemical exploration, and molecular modelling of the polyphenolic-rich fraction of Crepis sancta extract, Inflammopharmacology. 28 (2020) 321–331, https://doi.org/10.1007/s10787-019-00637-x.

[42] A. Waterhouse, M. Bertoni, S. Bienert, G. Studer, G. Tauriello, R. Gumienny, F. T. Heer, T.A.P. De Beer, C. Rempfer, L. Bordoli, R. Lepore, T. Schwede, SWISS-MODEL: Homology modelling of protein structures and complexes, Nucleic Acids Res. 46 (2018) W296–W303, https://doi.org/10.1093/nar/gky427.

[43] S.S. Ebada, N.A. Al-Jawabri, F.S. Youssef, D.H. El-Kashef, T.O. Knedel, A. Albohy, M. Korinek, T.L. Hwang, B.H. Chen, G.H. Lin, C.Y. Lin, S.M. Aldalaien, A.M. Disi, C. Janiak, P. Proksch, Anti-inflammatory, antiallergic and COVID-19 protease inhibitory activities of phytochemicals from the Jordanian hawksbeard: Identification, structure-Activity relationships, molecular modeling and impact on its folk medicinal uses, RSC Adv. 10 (2020) 38128–38141, https://doi.org/10.1039/d0ra04876c.

[44] J. Huang, A.D. Mackerell, CHARMM36 all-atom additive protein force field: Validation based on comparison to NMR data, J. Comput. Chem. 34 (2013) 2135–2145, https://doi.org/10.1002/jcc.23354.

[45] V. Zoete, M.A. Cuendet, A. Grosdidier, O. Michielin, SwissParam: A fast force field generation tool for small organic molecules, J. Comput. Chem. 32 (2011) 2359–2368, https://doi.org/10.1002/jcc.21816.

[46] P. Mark, L. Nilsson, Structure and dynamics of the TIP3P, SPC, and SPC/E water models at 298 K, J. Phys. Chem. A. 105 (2001) 9954–9960, https://doi.org/10.1021/jp003020w.

[47] M.J. Abraham, T. Murtola, R. Schulz, S. Páll, J.C. Smith, B. Hess, E. Lindah, Gromacs: High performance molecular simulations through multi-level parallelism from laptops to supercomputers, SoftwareX. 1–2 (2015) 19–25, https://doi.org/10.1016/j.softx.2015.06.001.

[48] G. Bussi, D. Donadio, M. Parrinello, Canonical sampling through velocity rescaling, J. Chem. Phys. 126 (2007), https://doi.org/10.1063/1.2408420.

[49] M. Parrinello, A. Rahman, Polymorphic transitions in single crystals: A new molecular dynamics method, J. Appl. Phys. 52 (1981) 7182–7190, https://doi.org/10.1063/1.328693.

[50] T. Darden, D. York, L. Pedersen, Particle mesh Ewald: An N·log(N) method for Ewald sums in large systems, J. Chem. Phys. 98 (1993) 10089–10092, https://doi.org/10.1063/1.464397.

[51] R. Kumari, R. Kumar, A. Lynn, G-mmpbsa -A GROMACS tool for high-throughput MM-PBSA calculations, J. Chem. Inf. Model. 54 (2014) 1951–1962, https://doi.org/10.1021/ci500020m.